

# A linear model of elasto-plastic and adhesive contact deformation

Massih Pasha · Selasi Dogbe · Colin Hare ·  
Ali Hassanpour · Mojtaba Ghadiri

Received: 6 November 2012 / Published online: 19 January 2014  
© The Author(s) 2014. This article is published with open access at Springerlink.com

**Abstract** Rigorous non-linear models of elasto-plastic contact deformation are time-consuming in numerical calculations for the distinct element method (DEM) and quite often unnecessary to represent the actual contact deformation of common particulate systems. In this work a simple linear elasto-plastic and adhesive contact model for spherical particles is proposed. Plastic deformation of contacts during loading and elastic unloading, accompanied by adhesion are considered, for which the pull-off force increases with plastic deformation. Considering the collision of a spherical cohesive body with a rigid flat target, the critical sticking velocity and coefficient of restitution in the proposed model are found to be very similar to those of Thornton and Ning's model. Sensitivity analyses of the model parameters such as plastic, elastic, plastic-adhesive stiffnesses and pull-off force on work of compaction are carried out. It is found that by increasing the ratio of elastic to plastic stiffness, the plastic component of the total work increases and the elastic component decreases. By increasing the interface energy, the plastic work increases, but the elastic work does not change. The model can be used to efficiently represent the force-displacement of a wide range of particles, thus enabling fast numerical simulations of particle assemblies by the DEM.

**Keywords** Distinct element model (DEM) · Contact force model · Cohesive powder · Plastic deformation · Coefficient of restitution · Normal impact · Adhesion

## 1 Introduction

The macroscopic bulk behaviour of powders is governed by the microscopic activity of the individual particles in an assembly. This implies that in order to gain a better understanding of particulate systems and their functioning, the particle interactions at the microscopic level must be analysed. It is currently very difficult to investigate the behaviour of individual particles within a bulk assembly experimentally. Therefore it is helpful to model the behaviour of particles by the use of numerical simulations. Furthermore the use of computer simulations provides a cost effective method as an alternative to experiments, since no physical material or process equipment is required, provided the simulation results are validated. Simulations are also invaluable for cases for which actual experiments are hazardous. For particulate solids, the most appropriate approach for this purpose is the use of computer simulation by the distinct element method (DEM). More details on the methodology of the DEM and its applications are presented elsewhere [1,2]. Various contact models have been proposed in the literature for evaluation of forces arising from inter-particle collisional interactions. Ning [3] categorized the factors involved in a single contact into three main categories: impact parameters such as particle velocity and impact angle, particle properties such as size, shape, density, surface friction, adhesion and roughness, and environmental factors such as temperature. Considering such a wide range of factors involved in the interactions, modelling of inter-particle contacts is a particularly complex process. Various contact models have been developed and reported in the literature for elastic [1,4–6], elastic-adhesive [7–13], elasto-plastic [14–17] and elasto-plastic and adhesive [18–21] contacts, some of which involve complex mathematical equations. The more complex a model, the slower the simulations. Simplifications can be done in order to reduce

M. Pasha · S. Dogbe · C. Hare · A. Hassanpour · M. Ghadiri (✉)  
Institute of Particle Science and Engineering,  
University of Leeds, Leeds LS2 9JT, UK  
e-mail: M.Ghadiri@leeds.ac.uk

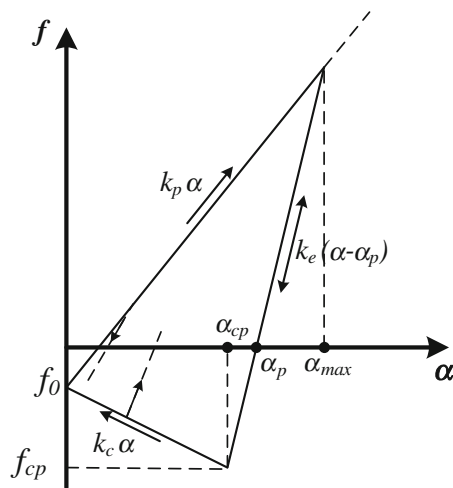


**Fig. 1** Schematic diagram of force-overlap relationship in Luding's [20] model

the computational complexity of the models; however this comes at the expense of losing the accuracy of capturing the realistic behaviour. In the present work a model is proposed considering aspects of Thornton and Ning's [18], Tomas's [19], and Walton and Johnson's [21] models. Sensitivity analyses of the proposed model parameters on bulk compaction behaviour are also reported.

In the following an overview of the available linear models reported in the literature for elasto-plastic and adhesive contact deformation is presented.

#### Luding's model [20]:

Figure 1 illustrates schematically the normal contact model of Luding [20] for elasto-plastic and adhesive contacts. In this model, the normal force will drop to a certain negative value,  $f_0$ , when two spheres come into contact due to van der Waals attractive forces [8–10]. On initial compression loading, the contact is considered to be plastically deforming; the contact force increases linearly with the overlap  $\alpha$  at a rate  $k_p$  (i.e. plastic stiffness) until an overlap  $\alpha_{max}$  is reached ( $\alpha_{max}$  is kept in memory as a history variable). During unloading the force drops on a line with the elastic stiffness (slope)  $k_e$ . The force decreases to zero at overlap  $\alpha_p$ , which represents the plastic contact deformation. Reloading at any instant leads to an increase of the force along the same line with slope  $k_e$ , until the previous maximum force is reached; if  $\alpha$  increases further beyond  $\alpha_{max}$ , the force again follows the line with plastic stiffness (slope)  $k_p$  and  $\alpha_{max}$  has to be adjusted accordingly. Unloading below  $\alpha_p$  produces an adhesive force until the maximum tensile force,  $f_{cp}$ , is reached at overlap  $\alpha_{cp}$ . Further unloading leads to a reduction in the attractive force on the adhesive branch with a negative “stiffness” (slope)  $k_c$ . The maximum tensile force in this model increases by having larger deformations, i.e. increasing  $\alpha_{max}$  results in

a larger negative  $f_{cp}$ . This is a linear simplification of the so-called adhesion limit as defined by Tomas [22,23]. Similarly, Thornton and Ning [18] modelled the pull-off force to overcome the adhesion based on the increase in radius of curvature of the contact area: the unloading path in Thornton and Ning's model is considered to follow the JKR equation but with a larger radius of curvature due to plastic deformation. Luding [20] considered an elastic stiffness,  $k_e$ , which increased with the maximum overlap based on the work of Walton and Braun [14]. For overlaps greater than  $\alpha^*$ , elastic stiffness is equal to  $\hat{k}_e$  and for smaller overlaps the elastic stiffness is evaluated by:

$$k_e = k_p + \left( \hat{k}_e - k_p \right) \frac{\alpha_{max}}{\alpha^*} \quad (1)$$

The plastic flow limit overlap,  $\alpha^*$ , i.e. the overlap beyond which the elastic stiffness becomes independent of the maximum overlap, was defined by:

$$\alpha^* = \frac{\hat{k}_e}{\hat{k}_e - k_p} \phi_f 2R^*, \quad (2)$$

where  $\hat{k}_e$  is the maximum value of the elastic stiffness,  $\phi_f$  is the dimensionless plasticity depth and  $R^*$  is the reduced radius given by:

$$R^* = \left( \frac{1}{R_1} + \frac{1}{R_2} \right)^{-1}, \quad (3)$$

where  $R_1$  and  $R_2$  are the radii of the spheres in contact.

Luding's model contains a shortcoming by which the behaviour of elasto-plastic and adhesive contacts is not realistically simulated. Contacts “break” at zero overlap ( $\alpha = 0$ ), regardless of loading or unloading history. This implies that plastic deformation has been ignored, which is unrealistic since plastic deformation is permanent and hence detachment must take place at  $\alpha > 0$ .

#### Walton and Johnson's model [21]:

This model is shown schematically in Fig. 2 and accounts for plastic deformation. In this model, the contact starts at  $\alpha = 0$  with a normal contact force of zero, unlike the models of Thornton and Ning, Luding (with  $f_0 \neq 0$ ) and Tomas, where a small tensile force is assumed to exist at the point of contact due to the molecular attractions between the two bodies in contact. In Walton and Johnson's model [21], if the particles in contact are to be separated just at the point of first contact, the contact detachment does not occur until a separation distance of  $\alpha_{fe}$ . This behaviour is analogous to the JKR theory of work of adhesion: the work required to break an elastic and adhesive contact is larger than that which is used to bring them together. Similar to Luding's

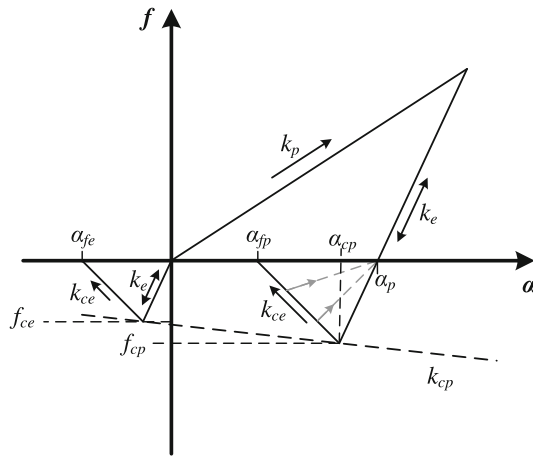


**Fig. 2** Schematic force-overlap response according to Walton and Johnsons' model [21]

model, under compressive loading the contact is assumed to deform plastically with a linear stiffness of  $k_p$ . The contact unloading follows the line with slope  $k_e$  until the unloading path intercepts with the locus of the pull-off force at  $f_{cp}$ . Contact reloading before the unloading reaches the pull-off force  $f_{cp}$  follows the unloading path. Further unloading beyond this point follows a path with negative slope  $k_{ce}$ , until the contact breaks when the force reaches zero at  $\alpha_{fp}$ . A linear locus (dashed line) is considered for the pull-off force with a negative slope of  $k_{cp}$ . However if the contact is reloaded after unloading beyond the pull-off force (i.e. reloading on  $k_{ce}$  branch), the contact force is evaluated based on a stiffness whose response provides a line from the point of reloading to  $\alpha_p$  (see the two reloading responses in Fig. 2 denoted by grey dashed lines), from where further reloading follows the elastic  $k_e$  line.

## 2 The proposed contact model

The proposed model is a linear elasto-plastic adhesive model with the detachment condition governed by the work of adhesion, and the normal force-overlap response shown in Fig. 3. Similar to the models of Luding, Tomas and Thornton and Ning, the normal force drops to a certain negative value,  $f_0$ , when two spheres come into contact at  $\alpha = 0$  due to van der Waals attractive forces. The contact is assumed to be elastically deforming for  $\alpha < \alpha_y$ . For  $\alpha \geq \alpha_y$  the contact deformation is elasto-plastic until point  $D$ . The initial elastic deformation is considered to be a linear version of JKR: the tensile force  $f_0$  is equal to  $8f_{ce}/9$ , where  $f_{ce}$  is the JKR elastic pull-off force (point  $B$ ) given by Eq. (4),

$$f_{ce} = -\frac{3}{2}\pi R^* \Gamma \quad (4)$$

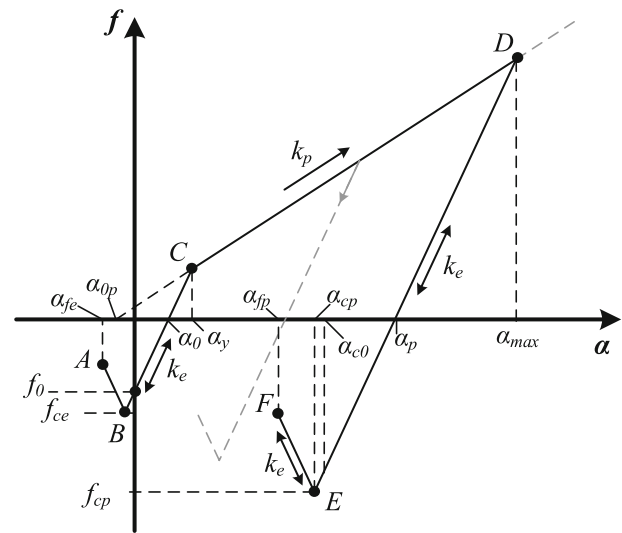


**Fig. 3** Schematic diagram of the normal force-overlap relationship in the proposed model

where  $\Gamma$  is the interface energy. The contact is assumed to be elastically deforming with an elastic stiffness,  $k_e$ , for line  $BC$ , for which the contact force is given by Eq. (5),

$$f = k_e \alpha + \frac{8}{9} f_{ce} \quad (5)$$

Since the deformation is elastic, the unloading curve follows the same path on the  $BC$  line. Unloading beyond point  $B$  is governed by a “stiffness”  $-k_e$ . The contact breaks at a negative overlap,  $\alpha_{fe}$ , at point  $A$  with the contact force being  $5f_{ce}/9$ .

On compressive loading beyond  $\alpha_y$  the contact reaches the yield stress and plastic deformation takes place which is governed by the plastic stiffness,  $k_p$ , on line  $CD$ .

$$f = k_p (\alpha - \alpha_{0p}) \quad (6)$$

The yielding force and deformation are given by Thornton [24] and Johnson [25]. Once the contact is unloaded from point  $D$ , the path lies on line from  $D$  to  $\alpha_p$  with elastic stiffness  $k_e$ , as given by:

$$f = k_e (\alpha - \alpha_p), \quad (7)$$

where  $\alpha_p$  is the overlap at which the unloading force becomes zero. The unloading path continues until a maximum tensile force ( $f_{cp}$ ), known as the pull-off force, is reached (point  $E$ ). The calculation of  $f_{cp}$  is provided in Sect. 2.1. For unloading beyond the pull-off force (line  $EF$ ), a negative elastic stiffness,  $-k_e$ , is considered. The governing equation for this part of contact force can be evaluated by Eq. (8),

$$f = -k_e (\alpha - 2\alpha_{cp} + \alpha_p) \quad (8)$$

where  $\alpha_{cp}$  is the overlap at which the pull-off force is achieved. The contact is considered to break at an overlap which provides a force equivalent to  $5f_{cp}/9$  similar to the JKR theory. Different from both previous models, deformations expressed by Eq. (8) are reversible, i.e. reloading follows the path of unloading, like for Eq. (7), and if reloading goes beyond point  $D$ , the deformation is plastic and follows Eq. (6). If the two bodies come towards each other again after the contact is broken, the contact is considered to be established at an overlap slightly larger than  $\alpha_{cp}$  (i.e.  $\alpha_{c0}$ ) by analogy with JKR theory, considering the surfaces relax following detachment. At this point the contact force is equal to  $8f_{cp}/9$ . The increasing elastic stiffness  $k_e$  due to increased maximum overlap, as suggested by Walton and Braun [14] and implemented by Luding [20], is adopted for the simplified model described later.

### 2.1 The load-dependent pull-off force

In order to account for the increase in the pull-off force due to plastic deformation (i.e. flattening of the contact area), the pull-off force is evaluated by applying an energy balance: the work of adhesion of the contacts is equated to  $A_p \Gamma$ , where  $A_p$  is the contact area of the plastic deformation. The plastic deformation (overlap),  $\alpha_{pd}$ , is given by:

$$\alpha_{pd} = \alpha_p - \alpha_y, \quad (9)$$

and the contact area can be estimated from the reduced radius of the sphere  $R^*$  and the overlap  $\alpha_{pd}$ , hence the work of adhesion is,

$$|W_{ad}| = A_p \Gamma = \pi \Gamma (2R^* \alpha_{pd} - \alpha_{pd}^2) \quad (10)$$

The work of adhesion is also the area under the unloading response from  $\alpha_p$  to  $\alpha_{fp}$  (Fig. 3), which can be derived to give (see Appendix I for the details of this derivation),

$$|W_{ad}| = \frac{137}{162} \frac{f_{cp}^2}{k_e} \quad (11)$$

By equating the right hand sides of Eqs. (10) and (11), and considering that the pull-off force is tensile, we get

$$f_{cp} = -\sqrt{\frac{162}{137} \pi \Gamma R^* k_e \alpha_{pd} \left(2 - \frac{\alpha_{pd}}{R^*}\right)} \quad (12)$$

as an expression for the pull-off force as a function of  $\alpha_{pd}$ . However it is of interest to show the locus of the pull-off force, hence  $f_{cp}$  is expressed in terms of  $\alpha_{cp}$  in Fig. 4 for the case where  $k_e = 1,500$  N/m,  $k_p = 210$  N/m,  $\Gamma = 0.02$  J/m<sup>2</sup> and  $R^* = 2.45$   $\mu$ m. The selection of these values is explained in Sect. 3.

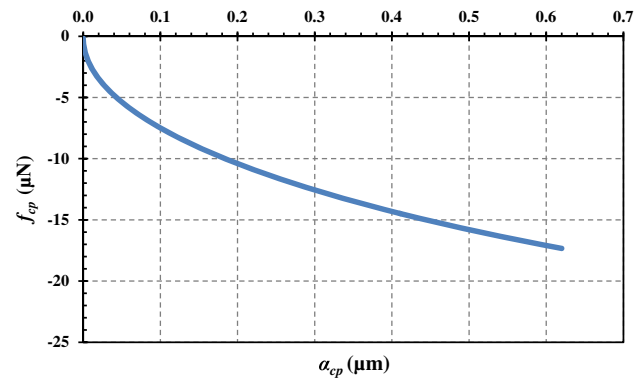


Fig. 4 Pull-off force as a function of  $\alpha_{cp}$

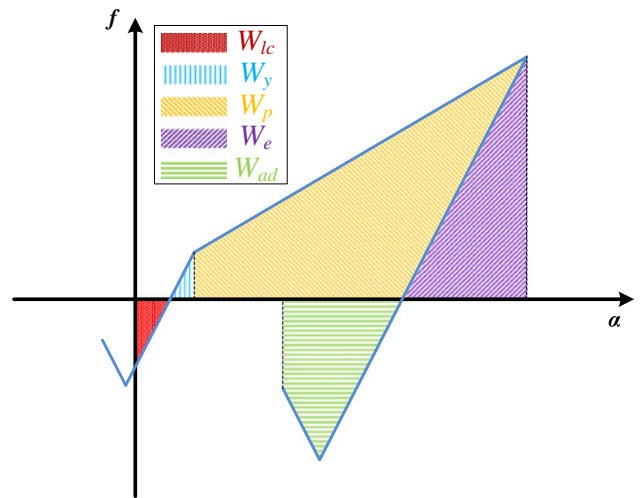


Fig. 5 Schematic force-overlap response of the proposed model and corresponding work of deformation

The magnitude of pull-off force increases with plastic deformation initially very rapidly and then more linearly, an observation which is also present in the elasto-plastic and adhesive models of Thornton and Ning [18], Tomas [19], Luding [20], and Walton and Johnson [21].  $\alpha_{cp}$  is directly related to  $\alpha_p$ , for which a similar functional relationship prevails.

### 2.2 Impact, rebound and critical sticking velocities

In this section, the equations for the impact, rebound and critical sticking velocity are derived based on applying an energy balance during contact loading and unloading. The force-overlap response of the proposed model is shown schematically in Fig. 5. Different areas under the response lines, corresponding to different energies, are shaded and coloured.  $W_{lc}$ ,  $W_y$ ,  $W_p$ ,  $W_e$  and  $W_{ad}$  correspond to the initial loading adhesive work, elastic compressive work until the yield point, plastic work, elastic unloading work and

work of adhesion, respectively. Considering the impact of a sphere against a large rigid body with a flat surface, the energy balance from the point where the contact is first made to where the velocity becomes zero is given by  $E_i$ ,

$$E_i = \frac{1}{2} m v_i^2 = W_p + W_e + W_y - |W_{lc}| \quad (13)$$

where  $v_i$  is the impact velocity. The elastic strain energy,  $W_e$ , is responsible for the rebound. There exists a critical balance between  $W_e$  and  $W_{ad}$  which determines whether the sphere sticks or rebounds. The critical sticking velocity,  $v_s$ , is the maximum impact velocity at which the contact does not break, where the energy of adhesion cannot be overcome by the elastic strain energy. Hence,

$$W_e = |W_{ad}| \rightarrow v_i = v_s \quad (14)$$

For impact velocities larger than  $v_s$ , the unloading leads to detachment of the contact. The rebound velocity,  $v_r$ , can be derived based on the following energy balance,

$$E_r = \frac{1}{2} m v_r^2 = W_e - |W_{ad}| \quad (15)$$

where  $E_r$  is the rebound kinetic energy. The rebound velocity derived from Eq. (15) is given by Eq. (16),

$$v_r = \left( f_{\max} \frac{(\alpha_{\max} - \alpha_p)}{m} - \frac{137}{81} \frac{f_{cp}^2}{m k_e} \right)^{1/2} \quad (16)$$

and Eq. (13) can be re-arranged for an expression in terms of  $v_i$  (Eq. 17), based on which the coefficient of restitution, i.e. the ratio of  $v_r$  to  $v_i$  can be calculated. Details of these derivations are provided in Appendix II.

$$v_i = \left( \frac{(f_{\max} + f_y)(\alpha_{\max} - \alpha_y) + (\alpha_y - \alpha_0) f_y - \alpha_0 |f_0|}{m} \right)^{1/2} \quad (17)$$

Figures 6, 7 and 8 show the coefficient of restitution as a function of impact velocity for different values of the interface energy, elastic and plastic stiffnesses, respectively. In all cases the fixed properties are as follows:  $k_e = 1,500$  N/m,  $k_p = 210$  N/m,  $\Gamma = 0.02$  J/m<sup>2</sup>, and  $R = 2.45$   $\mu$ m. The selection of these values is explained in Sect. 4. The critical sticking velocities are given in captions of Figs. 6, 7 and 8.

The coefficient of restitution reaches an asymptote at very high impact velocities. The asymptotic value is a function of contact properties. Increasing the interface energy results in a reduction of the coefficient of restitution since the cohesion is increased. Increasing the elastic stiffness also reduces the coefficient of restitution, since the plastic work is increased.

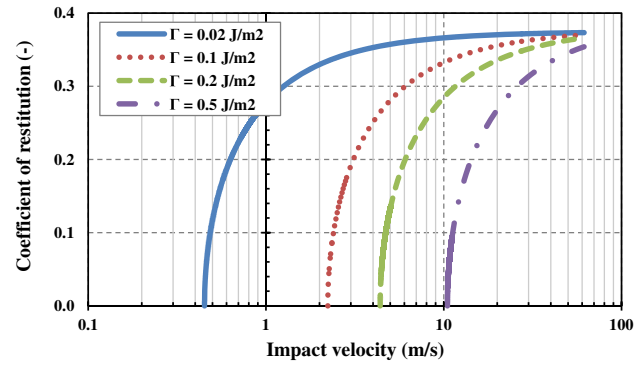


**Fig. 6** Coefficient of restitution as a function of impact velocity for different interface energies:  $k_e = 1,500$  N/m,  $k_p = 210$  N/m. The critical sticking velocity for the four data sets are 0.451, 2.228, 4.387 and 10.485 m/s

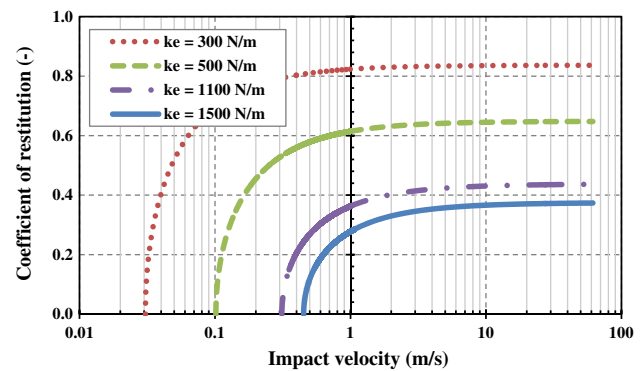


**Fig. 7** Coefficient of restitution as a function of impact velocity for different elastic stiffnesses:  $k_p = 210$  N/m,  $\Gamma = 0.02$  J/m<sup>2</sup>. The critical sticking velocity for the four data sets are 0.031, 0.102, 0.317 and 0.451 m/s

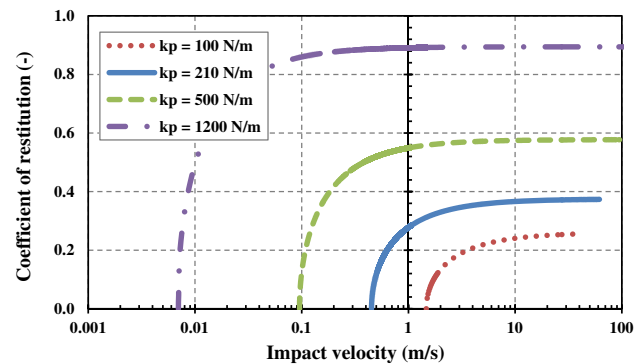


**Fig. 8** Coefficient of restitution as a function of impact velocity for different plastic stiffnesses:  $k_e = 1,500$  N/m,  $\Gamma = 0.02$  J/m<sup>2</sup>. The critical sticking velocity for the four data sets are 0.007, 0.095, 0.451 and 1.471 m/s

Increasing the plastic stiffness increases the coefficient of restitution, since the contact becomes stiffer and the extent of plastic deformation is reduced.



### 2.3 Linearization of the locus of pull-off force

Figure 4 showed that the locus of pull-off force for different extents of plastic deformation is governed by the specific surface energy and the flattened contact area. The locus is not linear at very small deformations, yet becomes linear towards large deformations, see Sect. 2.1; for more details see reference [26]. In an attempt to propose a more computationally cost-effective model, the locus of the pull-off force is considered to be only the linear part of the locus. Hence the pull-off force can be approximated as,

$$f_{cp} = -k_{cp}\alpha_{cp} + f_{0p} \quad (18)$$

where  $k_{cp}$  is the slope of the linear fit and  $f_{0p}$  is the intersection of the fit with the force-axis. The part of the pull-off force locus for large deformations (larger than 6 % of particle radius) and the linear fits for different interface energies are shown in Fig. 9.

Furthermore, in a number of cases the initial elastic deformation may be small as compared to the total deformation, as it is the case for materials with notable plastic deformation in which case the model can be simplified further. In real contacts, the presence of surface asperities always leads to plastic deformations right from the beginning of loading. If the initial elastic deformation is ignored, the force-overlap response can be simplified to the model that is shown schematically in Fig. 10. Once the contact is established at  $\alpha = 0$ , the contact force drops to a tensile force which is equivalent to  $8f_{ce}/9$ , where  $f_{ce}$  is the JKR pull-off force given by Eq. (4). The contact is plastically deformed on the line  $\alpha_0$  to  $B$  with force

$$f = k_p\alpha - \frac{8}{9}f_{ce} \quad (19)$$

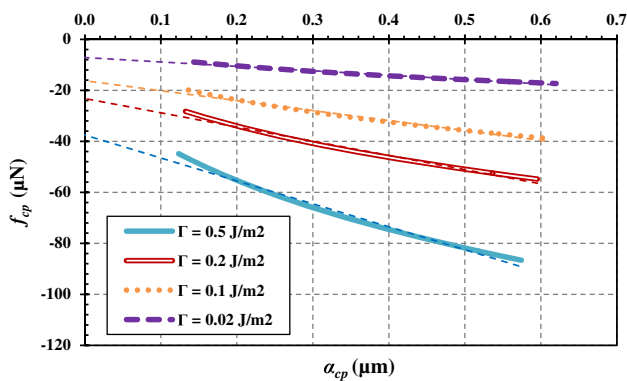


**Fig. 9** Pull-off force as a function of  $\alpha_{cp}$  for different interface energies:  $k_e = 1,500$  N/m,  $k_p = 210$  N/m, and  $R^* = 2.45$   $\mu\text{m}$ . The dashed lines are the fitted lines to the linear part of the loci given by Eq. 18 (i.e. deformation larger than 6 % of the particle radius)

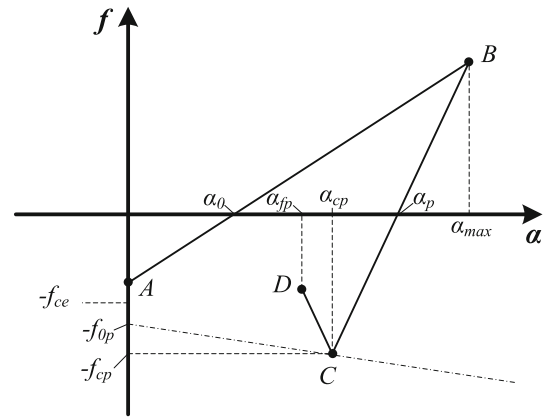


**Fig. 10** Schematic force-overlap response of the simplified model

The unloading curve lies on a line with the elastic stiffness  $k_e$  (line  $BC$ ), so that

$$f = k_e (\alpha - \alpha_p) \quad (20)$$

The unloading path continues until the pull-off force ( $f_{cp}$ ) is reached at

$$\alpha_{cp} = \frac{k_e\alpha_p - f_{0p}}{k_e + k_{cp}} \quad (21)$$

For unloading beyond the pull-off force (line  $CD$ ), a negative elastic stiffness,  $-k_e$ , is considered, leading to the contact force

$$f = -k_e (\alpha - 2\alpha_{cp} + \alpha_p) \quad (22)$$

The contact is considered to break at an overlap which provides a force equivalent to  $5f_{cp}/9$ , i.e. similar to the JKR theory. If the two bodies come towards each other again after the contact is broken, the contact is considered to be established at an overlap slightly larger than  $\alpha_{cp}$  (i.e.  $\alpha_{c0}$ ) in line with the previous model, see Fig. 3, representing surface relaxation following detachment. At this point the contact force is equal to  $8f_{cp}/9$ .

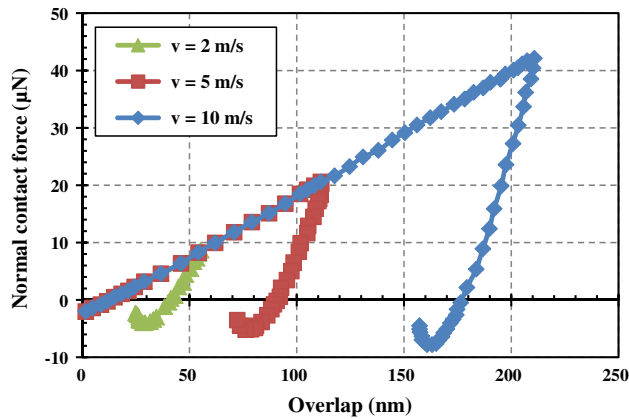
### 3 Comparison of the proposed model with that of Thornton and Ning [18]

Ning [3] simulated the impact of an ammonium fluorescein particle to a silicon target using Thornton and Ning's [18] model. The parameters in these simulations are summarized in Table 1.

The force-overlap responses with three different impact velocities of 2, 5 and 10 m/s are shown in Fig. 11. PlotDigitizer software was used to digitise the response in Fig. 11. In order to simulate the same system with the proposed models,

**Table 1** Properties of ammonium fluorescein particle and silicon wall used in Ning's [3] simulations

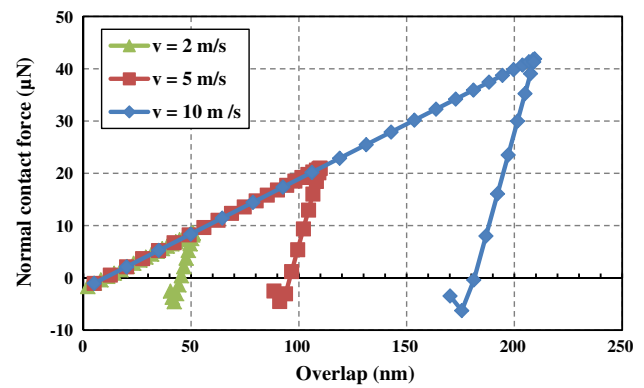
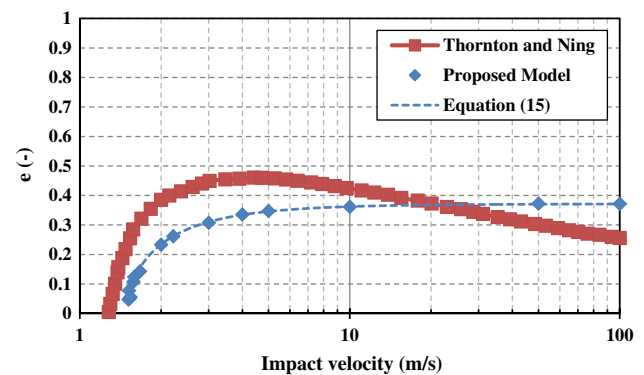
Property	Particle	Wall
Radius ( $\mu\text{m}$ )	2.45	—
Density ( $\text{kg/m}^3$ )	1,350	1,350
Elastic modulus (GPa)	1.2	182
Poisson's ratio (—)	0.3	0.3
Interface energy ( $\text{J/m}^2$ )	0.2	
Contact yield pressure (MPa)	35.3	

**Fig. 11** Normal force-overlap responses of impact of an ammonium fluorescein particle to a silicon target using Thornton and Ning's [18] model with three different impact velocities [3]. The data are obtained by digitizing the results of Thornton and Ning**Table 2** Model parameters obtained by determining the slopes of the responses in Fig. 11

$k_e$ (N/m)	1,500
$k_p$ (N/m)	210
$k_{cp}$ (N/m)	−20
$f_0$ ( $\mu\text{N}$ )	−2.1
$f_{0p}$ ( $\mu\text{N}$ )	−4.0

the elastic, plastic and adhesive stiffnesses are evaluated by determining the slopes of the responses from Fig. 11. The values are summarized in Table 2.

It is noteworthy that the elastic stiffness,  $k_e$ , in Table 2 is the average value of the initial unloading slopes in Fig. 11. The proposed simplified model with the linear pull-off force locus (shown in Fig. 9) was implemented as a subroutine for EDEM<sup>®</sup> software provided by DEM-Solutions, Edinburgh, UK. Using the parameters in Table 2, the impact of a 2.45  $\mu\text{m}$  radius sphere on a flat wall at three impact velocities of 2, 5 and 10 m/s was simulated, with no additional viscous/velocity dependent contact damping. The responses using the proposed model are shown in Fig. 12.

**Fig. 12** Normal force-overlap responses of impact of a 2.45  $\mu\text{m}$  radius particle to a wall with the parameters in Table 2 using the simplified proposed model for three different impact velocities**Fig. 13** Coefficient of restitution as a function of impact velocity using different contact models for a 2.45  $\mu\text{m}$  radius ammonium fluorescein particle impacting to a silicon target. The dashed line is obtained analytically by applying an energy balance as described in Sect. 3.2 and the data points with the marker (diamond) are from EDEM<sup>®</sup> software simulations

Comparing Figs. 11 and 12 a good agreement is observed between the simplified proposed model and that of Thornton and Ning in terms of the maximum overlap and permanent plastic deformation at different impact velocities.

In order to provide a more in depth comparison, the coefficient of restitution as a function of impact velocity was calculated from the impact and rebound velocities obtained from the numerical simulations data using EDEM<sup>®</sup> software as well as from the energy balance given by Eq. (15). The results for the 2.45  $\mu\text{m}$  radius ammonium fluorescein particle impacting at the silicon target are shown in Fig. 13 for these models. For the simplified proposed model, the data points are from the simulation data and the continuous curves are from the energy balance approach. For the Thornton and Ning model [18], the data are taken directly from Ning [3].

Figure 13 shows a reasonable agreement between the proposed model and that of Thornton and Ning given the simplification. The dotted lines are obtained analytically by applying an energy balance as described in Sect. 2.2. Since the

simulation results of the proposed model lie on the analytical curves, it can be concluded that the energy balance considerations in Sect. 2.2 are correct. The critical sticking velocity in the proposed model is very similar to that of Thornton and Ning ( $\sim 1.6$  m/s). With the proposed model, the coefficient of restitution increases initially, however it reaches an asymptotic value of  $\sim 0.38$  for impact velocities larger than about 10 m/s. The reason for this is attributed to a constant elastic stiffness, for which the ratio of elastic work ( $W_e$ ) to plastic work ( $W_p$ ) is always constant. At very high impact velocities, the elastic strain energy becomes very large relative to the work of adhesion ( $W_{ad}$ ), so the elasto-plastic process dominates since the plastic-cohesive stiffness,  $k_{cp}$ , is normally smaller than the plastic stiffness,  $k_p$ . Hence the asymptote has a value of  $(k_p/k_e)^{1/2}$  [14]. This asymptotic behaviour is not in line with the experimental evidence [27, 28], where it is shown that at sufficiently high velocity the impact energy far exceeds the adhesion energy and the coefficient of restitution is primarily a function of the energy loss due to plastic deformation.

In order to account for a decreasing coefficient of restitution at high impact velocities, the elastic unloading stiffness must be made load-dependent. Now, considering that the stiffness increases proportionally with the contact area, which in turn is a function of the maximum overlap,  $\alpha_{max}$ , the stiffness,  $k_e$ , is given by Eq. (23),

$$k_e \propto r^2 = 2R^*\alpha_{max} - \alpha_{max}^2 \quad (23)$$

where  $r$  is the contact radius. Assuming the maximum elastic stiffness,  $\hat{k}_e$ , is at an overlap of  $R^*$ , then

$$k_e = \left(\frac{r}{R^*}\right)^2 \hat{k}_e \quad (24)$$

For very small deformations, Eq. (24) gives elastic stiffness values which can be smaller than the plastic stiffness. In order to avoid such values for  $k_e$ , following the approach of Luding [20] as per Eq (1), Eq (24) can be modified as follows,

$$k_e = k_p + \left(\frac{r}{R^*}\right)^2 (\hat{k}_e - k_p) \quad (25)$$

The elastic stiffness can be evaluated by finding the tangent to the Hertz response of the contacts in Fig. 11 and finding the best match to the Hertz curve for initial stage of unloading. For the values given in Tables 1 and 2, a maximum elastic stiffness  $\hat{k}_e$  of 13,000 N/m was calculated using Eq. (25).

The coefficient of restitution as a function of impact velocity is shown in Fig. 14 for the proposed model with a load-dependent elastic unloading stiffness. This response is obtained by the same energy balance approach as described in Sect. 2.2. The prediction from Thornton and Ning's model is also given for comparison.

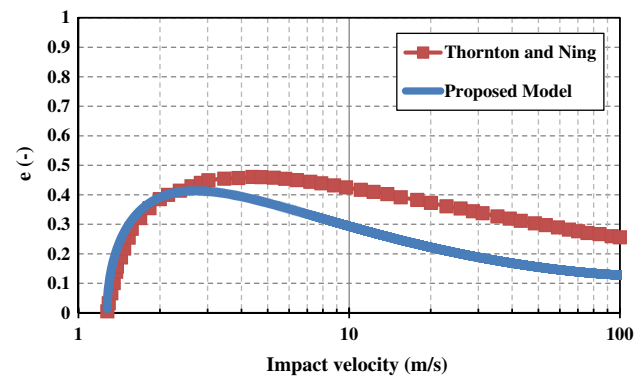


**Fig. 14** Coefficient of restitution as a function of impact velocity using the proposed model with a load-dependent unloading stiffness and Thornton and Ning model

As expected a decreasing coefficient of restitution is observed at high impact velocities, although showing a deviation from Thornton and Ning's model.

New experimental data are needed to check the validity of the model's predictions, as a larger data set than that available for ammonium fluorescein particles would provide more certainty.

There are clear differences between this model and those of Walton and Johnson [21] and Luding [20] in (1) the point of contact detachment, (2) reloading on the adhesive branch and (3) most importantly in the work of adhesion. The latter strongly influences the sticking velocity, as it depends on the balance between elastic strain energy and work of adhesion. Hence a rigorous test of these models is to experimentally verify the sticking velocity of materials, whose model parameters have been independently characterised.

#### 4 Sensitivity analysis of the proposed model parameters

A set of simulations were carried out in order to investigate the effects of the model parameters on the elastic and plastic components of work during loading and unloading of bulk compression. The tangential stiffness,  $k_t$ , was equated to the elastic stiffness,  $k_e$ , throughout the simulations. The model with a linear pull-off locus and with a constant unloading stiffness was used in these simulations. The model parameters for the particles are summarized in Table 3.

The sensitivity of bulk compression response to the plastic stiffness ( $k_p$ ) was evaluated with two fixed values of elastic stiffness,  $k_e$ , (1,000 and 5,000 N/m) in order to achieve the same stiffness ratio ( $k_e/k_p$ ) with different plastic stiffnesses. This facilitates the sensitivity analysis of stiffness ratio as well as sensitivity of elastic and plastic stiffnesses. The walls were considered to be elastic with zero adhesion (i.e.  $f_{01} = f_{0p} = 0$ ,  $k_{ce} = k_{cp} = 0$  and  $k_p = k_e = k_t$ ). The stiffness of the walls was set to be 8,000 kN/m. 3,400 particles with



**Table 3** Model parameter values used in the simulations

Parameter varied	$k_p$ (kN/m)	$k_e$ (kN/m)	$k_{cp}$ (kN/m)	$\Gamma$ (J/m <sup>2</sup> )
$k_e$	10	50, 100, 500, 1,000	0	0
$k_p$	10, 50, 100, 250, 500	1,000	0	0
$k_p$	50, 100, 500, 1,000, 2,500	5,000	0	0
$k_p = k_e$	100	100	0	0
$\Gamma$	100	1,000	5	0.05, 0.1, 1, 2, 5

**Table 4** Size distribution of the generated particles

Particle diameter (mm)	0.8	0.9	1	1.1	1.2
Number frequency (%)	5	25	40	25	5

a mean diameter of 1 mm and a normal size distribution (as shown in Table 4) were generated inside a cylindrical die of 12 mm diameter. This number of particles provided a bed height of approximately 36 mm. The density of the particles was set to be 1,000 kg/m<sup>3</sup>.

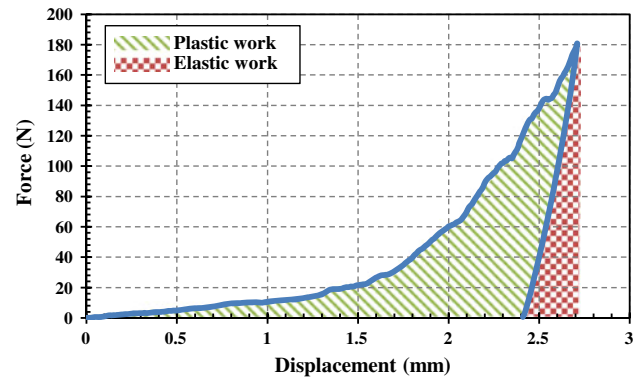
The time-step is calculated based on a mass-spring system as

$$t = 0.2t_{crit} = 0.2\sqrt{\frac{m^*}{k_{crit}^*}} \quad (26)$$

where  $t_{crit}$  is the critical time-step for a mass-spring system,  $m^* = m_{smallest}/2$  is the equivalent mass of the smallest particle, and  $k_{crit}^* = k_{smallest}/2$  is the largest equivalent stiffness in the system. The coefficient of sliding friction was 0.25 for both the particle–particle and particle–wall contacts. The compression was simulated at a strain rate of 0.28 s<sup>-1</sup>. In order to define the dynamics of the process, the dimensionless shear strain rate,  $\dot{\gamma}$ , of Tardos et al. [29] is evaluated using Eq. (27),

$$\dot{\gamma} = \gamma \left( \frac{d_p}{g} \right)^{1/2} \quad (27)$$

where  $\gamma$  is the shear strain rate,  $d_p$  is the mean particle diameter and  $g$  is the gravitational acceleration. The strain rate of 0.28 s<sup>-1</sup> provides a dimensionless shear strain rate of  $\sim 0.003$ . It is shown by Tardos et al. [29] that for dimensionless shear strain rates of  $< 0.15$ , the process is quasi-static, therefore the inertial effects on the stresses throughout the bulk are negligible. The assembly was compressed by moving the top platen until a bulk strain of 11 % (for non-cohesive cases) or a solid fraction of 0.58 (for cohesive cases) was achieved, after which the platen was unloaded with the same speed as the compression. The non-cohesive simulations all had very similar initial solid fractions and applying the same amount of strain produced similar final solid fractions. In

**Fig. 15** Typical loading–unloading curve of compaction ( $k_p = 10$  kN/m and  $k_e = 50$  kN/m)

contrast, the cohesive simulations provided different initial packing fractions since the cohesion was introduced prior to generation of particles, therefore the compression simulations were not strain-controlled and were run to the same final solid fractions. Figure 15 shows a typical force-displacement curve of the top platen during the bulk compression using EDEM<sup>®</sup> software.

The plastic work (i.e. irrecoverable work) on loading is calculated as the closed area underneath the curve (the green shaded area in Fig. 15). The elastic work (i.e. recoverable work) is calculated as the area underneath the unloading curve (the red hatched area in Fig. 15). The total input work is the addition of the plastic and elastic work components. The normalized elastic and plastic work components are defined as the elastic and plastic work, respectively, divided by the input work. Figure 16 shows the normalized elastic and plastic work components as a function of stiffness ratio,  $k_e/k_p$ , for all the cohesionless cases (first 4 rows of Table 3).

Large stiffness ratio values imply particles deforming extensively plastically, whereas a stiffness ratio of one implies a purely elastic deformation. For the stiffness ratio of one, the plastic component of the work is still larger than the elastic one. The plastic work in this case is due to particle rearrangements and frictional dissipation between the particles themselves and with the walls, since the normal contacts deform elastically. The graph shows that as the stiffness ratio increases, the fraction of plastic work increases, while that of elastic work decreases. The increase in the ratio means

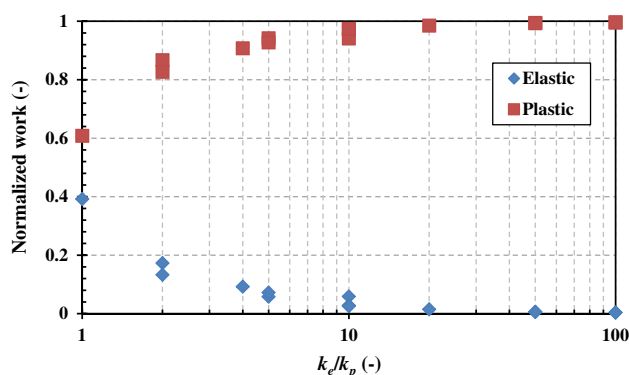


**Fig. 16** Normalized work as a function of stiffness ratio for all the cohesionless cases

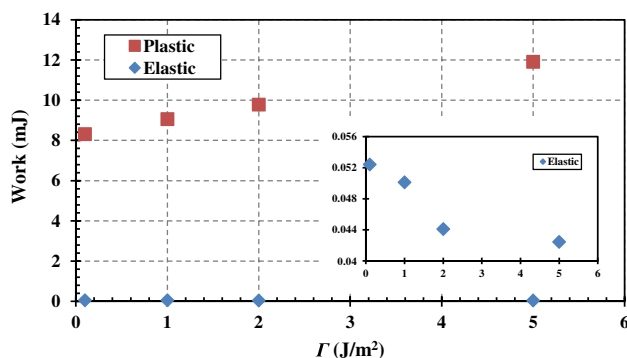


**Fig. 17** Elastic and plastic work components as a function of  $\Gamma$  ( $k_p = 100$  (kN/m),  $k_e = 1,000$  (kN/m),  $k_{cp} = -5$  kN/m)

either the plastic stiffness is decreased or the elastic stiffness is increased. If the plastic stiffness is decreased while the elastic stiffness is kept constant (softer particles), more work is expended in deforming contacts to reach the same force. This leads to an increase of the total work, while the elastic work remains the same. Therefore normalized elastic work decreases and normalized plastic work increases accordingly. In the case where the elastic stiffness is increased while plastic work is kept constant, the total input work does not change, but the fraction of elastic work decreases. This leads to a decrease in the normalized elastic work and consequently normalized plastic work increases. It can also be seen from Fig. 16 that there exists a limit for the stiffness ratio ( $k_e/k_p \approx 20$ ) beyond which almost all of the work input into the system is used in plastic deformation.

Figure 17 shows the plastic and elastic works as a function of increasing the interface energy. By increasing the interface energy, the plastic work increases; however the elastic work is very small for the range of  $\Gamma$  investigated here and it does not change significantly with the interface energy. This observation is attributed to the differences in the initial packing of the powder beds due to cohesion. This is shown in Fig. 18 as a function of the interface energy. As it can be seen, the initial solid fraction decreases with increasing interface energy. Therefore in order to get to the solid fraction of 0.58, more

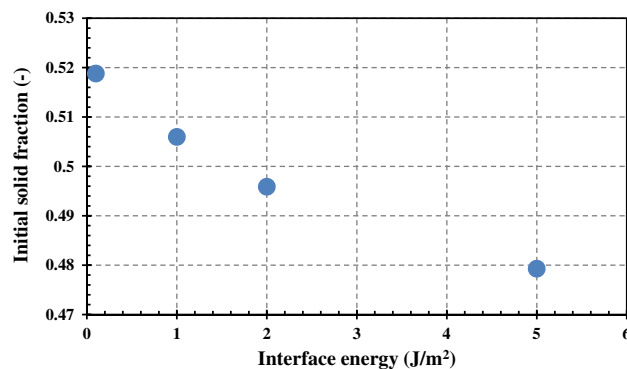


**Fig. 18** Initial solid fraction as a function of  $\Gamma$  ( $k_p = 100$  (kN/m),  $k_e = 1,000$  (kN/m),  $k_{cp} = -5$  kN/m)

cohesive beds will undergo higher strains, i.e. increasing the total input work.

## 5 Conclusions

A new linear elasto-plastic and adhesive contact model for spherical particles has been proposed based on the models of Luding [20] and Walton and Johnson [21] and considering aspects of Thornton and Ning's [18] and Tomas's [19] contact models. Plastic deformation of contacts during loading and pure elastic unloading, accompanied by adhesion are considered, for which the pull-off force increases with plastic deformation and for which the detachment is governed by the work of adhesion. Considering the collision of an adhesive spherical body with a rigid flat target, the critical impact velocity above which rebound occurs, as predicted by the proposed model, is found to be very similar to that of Thornton and Ning's model. This agreement is improved by considering a load-dependent unloading stiffness.

Sensitivity analyses of the model parameters on work of compaction reveal that by increasing the stiffness ratio ( $k_e/k_p$ ) the normalized plastic work increases and the normalized elastic work decreases. By increasing the interface energy, the plastic work increases, however the elastic work does not change notably. This highlights the flexibility of the model in representing the mechanical behaviour of a wide range of particulate materials. The linear nature of the model leads to time efficient simulations, whilst still capturing the complex material behaviour.

**Acknowledgments** The financial support of the Engineering and Physical Sciences Research Council, UK, through the Grant EP/G013047 is gratefully acknowledged. The authors are also grateful to the constructive critical comments of Professor Stefan Luding and the reviewers.

**Open Access** This article is distributed under the terms of the Creative Commons Attribution License which permits any use, distribution, and reproduction in any medium, provided the original author(s) and the source are credited.

## Appendix I: Derivation of work of adhesion

The work of adhesion is the negative area underneath the unloading curve (see Fig. 3), which consists of a triangle (with area of  $|W_{c1}|$ ) and a trapezoid (with area of  $|W_{c2}|$ ), hence,

$$|W_{ad}| = |W_{c1}| + |W_{c2}| \quad (28)$$

The triangle area  $|W_{c1}|$  is,

$$|W_{c1}| = \frac{1}{2} (\alpha_p - \alpha_{cp}) |f_{cp}|, \quad (29)$$

where  $\alpha_{cp}$  can be derived as follows,

$$\begin{aligned} @\alpha_{cp} : -|f_{cp}| &= k_e (\alpha_{cp} - \alpha_p) \\ \Rightarrow \alpha_{cp} &= \alpha_p - \frac{|f_{cp}|}{k_e} \end{aligned} \quad (30)$$

Substituting Eq. (30) into (29) gives,

$$\begin{aligned} |W_{c1}| &= \frac{1}{2} \left( \alpha_p - \alpha_p + \frac{|f_{cp}|}{k_e} \right) |f_{cp}| \\ \Rightarrow |W_{c1}| &= \frac{1}{2} \frac{|f_{cp}|^2}{k_e} \end{aligned} \quad (31)$$

The trapezoid area  $|W_{c2}|$  is,

$$\begin{aligned} |W_{c2}| &= \frac{1}{2} (\alpha_{cp} - \alpha_{fp}) \left( |f_{cp}| + \frac{5}{9} |f_{cp}| \right) \\ \Rightarrow |W_{c2}| &= \frac{7}{9} |f_{cp}| (\alpha_{cp} - \alpha_{fp}) \end{aligned} \quad (32)$$

Substituting Eq. (30) into (32) gives,

$$|W_{c2}| = \frac{7}{9} |f_{cp}| \left( \alpha_p - \frac{|f_{cp}|}{k_e} - \alpha_{fp} \right) \quad (33)$$

$\alpha_{fp}$  is derived as follows,

$$\begin{aligned} @\alpha_{fp} : -k_e (\alpha_{fp} - 2\alpha_{cp} + \alpha_p) &= -\frac{5}{9} |f_{cp}| \\ \Rightarrow \alpha_{fp} &= 2\alpha_{cp} - \alpha_p + \frac{5}{9} \frac{|f_{cp}|}{k_e} \end{aligned} \quad (34)$$

Substituting Eq. (30) into (34) gives,

$$\begin{aligned} \alpha_{fp} &= 2 \left( \alpha_p - \frac{|f_{cp}|}{k_e} \right) - \alpha_p + \frac{5}{9} \frac{|f_{cp}|}{k_e} \\ \Rightarrow \alpha_{fp} &= \alpha_p - \frac{13}{9} \frac{|f_{cp}|}{k_e} \end{aligned} \quad (35)$$

Substituting Eq. (35) into (33) gives,

$$\begin{aligned} |W_{c2}| &= \frac{7}{9} |f_{cp}| \alpha_p - \frac{7}{9} \frac{|f_{cp}|^2}{k_e} - \frac{7}{9} |f_{cp}| \\ &\times \left( \alpha_p - \frac{13}{9} \frac{|f_{cp}|}{k_e} \right) \Rightarrow |W_{c2}| = \frac{28}{81} \frac{|f_{cp}|^2}{k_e} \end{aligned} \quad (36)$$

Substituting Eqs. (31) and (36) into (28) gives,

$$|W_{ad}| = \frac{1}{2} \frac{|f_{cp}|^2}{k_e} + \frac{28}{81} \frac{|f_{cp}|^2}{k_e} \Rightarrow |W_{ad}| = \frac{137}{162} \frac{|f_{cp}|^2}{k_e} \quad (37)$$

## Appendix II: Derivation of impact and rebound velocities

The force-overlap response of the proposed model is shown schematically in Fig. 19. Different areas under the response lines, corresponding to different energies, are shaded and coloured.  $W_{lc}$ ,  $W_y$ ,  $W_p$ ,  $W_e$  and  $W_{ad}$  correspond to the initial loading adhesive work, elastic compressive work until the yield point, plastic work, elastic unloading work and work of adhesion, respectively.

The equations of these energies are derived as follows,  $W_{lc}$ :

$$|W_{lc}| = \frac{1}{2} \alpha_0 |f_0| \quad (38)$$

$W_y$ :

$$W_y = \frac{1}{2} (\alpha_y - \alpha_0) f_y \quad (39)$$

$W_e$ :

$$W_e = \frac{1}{2} f_{\max} (\alpha_{\max} - \alpha_p) \quad (40)$$

$W_p$  consists of a trapezoid with area of  $W_{p1}$  and a triangle with area of  $W_{p2}$ :

$$W_p = W_{p1} + W_{p2} \quad (41)$$

The trapezoid area is,

$$W_{p1} = \frac{1}{2} (f_y + f_p) (\alpha_p - \alpha_y) \quad (42)$$

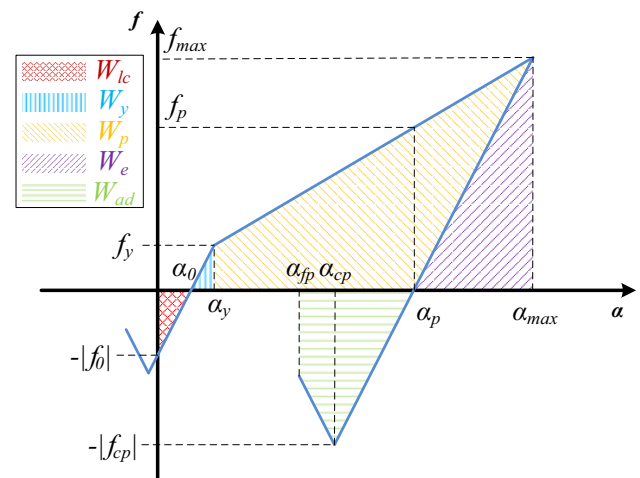


**Fig. 19** Schematic force-overlap response of the proposed model and corresponding work of deformation

The triangle area is,

$$\Rightarrow W_{p2} = \frac{1}{2} f_p (\alpha_{\max} - \alpha_p) \quad (43)$$

Substituting Eqs. (42) and (43) in (41) gives,

$$W_p = \frac{1}{2} (f_y + f_p) (\alpha_p - \alpha_y) + \frac{1}{2} f_p (\alpha_{\max} - \alpha_p) \quad (44)$$

$W_{ad}$  is given by Eq. (37).

Considering the impact of a sphere against a large rigid body with a flat surface, the energy balance from the point where the contact is first made to where the velocity becomes zero is given by  $E_i$ ,

$$E_i = \frac{1}{2} m v_i^2 = W_p + W_e + W_y - |W_{lc}| \quad (45)$$

where  $v_i$  is the impact velocity. Substituting Eqs. (38)–(41) into (45) gives,

$$\begin{aligned} \frac{1}{2} m v_i^2 &= \frac{1}{2} (f_{\max} + f_y) (\alpha_{\max} - \alpha_y) + \frac{1}{2} (\alpha_y - \alpha_0) f_y \\ &\quad - \frac{1}{2} \alpha_0 |f_0| \Rightarrow v_i \\ &= \left( \frac{(f_{\max} + f_y) (\alpha_{\max} - \alpha_y) + (\alpha_y - \alpha_0) f_y - \alpha_0 |f_0|}{m} \right)^{1/2} \end{aligned} \quad (46)$$

For impact velocities larger than the critical sticking velocity, the unloading leads to detachment of the contact. The rebound velocity,  $v_r$ , can be derived based on the following energy balance,

$$E_r = \frac{1}{2} m v_r^2 = W_e - |W_{ad}| \quad (47)$$

where  $E_r$  is the rebound kinetic energy. Substituting Eqs. (40) and (37) into (47) gives,

$$\begin{aligned} \frac{1}{2} m v_r^2 &= \frac{1}{2} f_{\max} (\alpha_{\max} - \alpha_p) - \frac{137 |f_{cp}|^2}{162 k_e} \\ \Rightarrow v_r &= \left( f_{\max} \frac{(\alpha_{\max} - \alpha_p)}{m} - \frac{137 |f_{cp}|^2}{81 m k_e} \right)^{1/2} \end{aligned} \quad (48)$$

## References

1. Cundall, P.A., Strack, O.D.L.: A discrete numerical model for granular assemblies. *Geotechnique* **29**, 47–65 (1979)
2. Zhu, H.P., Zhou, Z.Y., Yang, R.Y., Yu, A.B.: Discrete particle simulation of particulate systems: theoretical developments. *Chem. Eng. Sci.* **62**, 3378–3396 (2007)
3. Ning, Z.: Elasto-Plastic Impact of Fine Particles and Fragmentation of Small Agglomerates. PhD Thesis, Aston University (1995)
4. Hertz, H.: Über die Berührung fester elastischer Körper. *Journal für die reine und angewandte Mathematik* **92**, 156–171 (1882)
5. Di Renzo, A., Di Maio, F.P.: Comparison of contact-force models for the simulation of collisions in DEM-based granular flow codes. *Chem. Eng. Sci.* **59**, 525–541 (2004)
6. Thornton, C., Cummins, S.J., Cleary, P.W.: An investigation of the comparative behaviour of alternative contact force models during elastic collisions. *Powder Technol.* **210**, 189–197 (2011)
7. Thornton, C., Yin, K.K.: Impact of elastic spheres with and without adhesion. *Powder Technol.* **65**, 153–166 (1991)
8. Johnson, K.L., Kendall, K., Roberts, A.D.: Surface energy and the contact of elastic solids. *Proc. R Soc. A* **324**, 301–313 (1971)
9. Krupp, H.: Particle adhesion theory and experiment. *Adv. Colloid Interface Sci.* **1**, 111–239 (1967)
10. Derjaguin, B.V., Muller, V.M., Toporov, Y.P.: Effect of contact deformation on the adhesion of particles. *J. Colloid Interface Sci.* **53**, 314–326 (1975)
11. Yen, K.Z.Y., Chaki, T.K.: A dynamic simulation of particle rearrangement in powder packings with realistic interactions. *J. Appl. Phys.* **71**, 3164–3173 (1992)
12. Yang, R.Y., Zou, R.P., Yu, A.B.: Computer simulation of the packing of fine particles. *Phys. Rev. E* **62**, 3900–3908 (2000)
13. Israelachvili, J.N.: *Intermolecular and Surface Forces*. Academic Press, London (1991)
14. Walton, O.R., Braun, R.L.: Viscosity, granular-temperature, and stress calculations for shearing assemblies of inelastic, frictional disks. *J. Rheol.* **30**, 949–980 (1986)
15. Thornton, C., Cummins, S.J., Cleary, P.W.: An investigation of the comparative behaviour of alternative contact force models during inelastic collisions. *Powder Technol.* **233**, 30–46 (2013)
16. Thornton, C.: Coefficient of restitution for collinear collisions of elastic perfectly plastic spheres. *ASME J. Appl. Mech.* **64**, 383–386 (1997)
17. Vu-Quoc, L., Zhang, X.: An elastoplastic contact force–displacement model in the normal direction, displacement-driven version. *Proc. R Soc. Lond. Ser. A Math. Phys. Eng. Sci.* **455**, 4013–4044 (1999)
18. Thornton, C., Ning, Z.: A theoretical model for the stick/bounce behaviour of adhesive elastic–plastic spheres. *Powder Technol.* **99**, 154–162 (1998)
19. Tomas, J.: Fundamentals of cohesive powder consolidation and flow. *Granul. Matter* **6**, 75–86 (2004)
20. Luding, S.: Cohesive, frictional powders: contact models for tension. *Granul. Matter* **10**, 235–246 (2008)
21. Walton, O.R., Johnson, S.M.: Simulating the effects of interparticle cohesion in micron-scale powders. *AIP Conf. Proc.* **1145**, 897–900 (2009)
22. Tomas, J.: Adhesion of ultrafine particles—a micromechanical approach. *Chem. Eng. Sci.* **62**, 1997–2010 (2007)
23. Tomas, J.: Adhesion of ultrafine particles—energy absorption at contact. *Chem. Eng. Sci.* **62**, 5925–5939 (2007)
24. Thornton, C.: Coefficient of restitution for collinear collisions of elastic-perfectly plastic spheres. *J. Appl. Mech. Trans. ASME* **64**, 383–386 (1997)
25. Johnson, K.L.: *Contact Mechanics*. Cambridge University Press, Cambridge (1985)
26. Pasha, M.: Modelling of Flowability Measurement of Cohesive Powders Using Small Quantities. PhD Thesis, The University of Leeds (2013)
27. Wall, S., John, W., Wang, H., Goren, S.L.: Measurements of kinetic energy loss for particles impacting surfaces. *Aerosol Sci. Technol.* **12**, 926–946 (1990)
28. Kharaz, A.H., Gorham, D.A.: A study of the restitution coefficient in elastic-plastic impact. *Philos. Mag. Lett.* **80**, 549–559 (2000)
29. Tardos, G.I., McNamara, S., Talu, I.: Slow and intermediate flow of a frictional bulk powder in the Couette geometry. *Powder Technol.* **131**, 23–39 (2003)